Journal of Electron Spectroscopy and Related Phenomena 201 (2015) 115–120

Contents lists available at ScienceDirect

Journal of Electron Spectroscopy and Related Phenomena

journal homepage: www.elsevier.com/locate/elspec

Bulk and surface band structure of the new family of semiconductors BiTeX (X=I, Br, Cl)

L. Moreschini[a,*], G. Autès[b], A. Crepaldi[c], S. Moser[a,c], J.C. Johannsen[c], K.S. Kim[a,d,e], H. Berger[c], Ph. Bugnon[c], A. Magrez[c], J. Denlinger[a], E. Rotenberg[a], A. Bostwick[a], O.V. Yazyev[b], M. Grioni[c]

[a] Advanced Light Source (ALS), Lawrence Berkeley National Laboratory, Berkeley, CA 94720, USA
[b] Institute of Theoretical Physics, Ecole Polytechnique Fédérale de Lausanne (EPFL), CH-1015 Lausanne, Switzerland
[c] Institute of Condensed Matter Physics, Ecole Polytechnique Fédérale de Lausanne (EPFL), CH-1015 Lausanne, Switzerland
[d] Department of Physics, Pohang University of Science and Technology, Pohang 790-784, Republic of Korea
[e] Center for Artificial Low Dimensional Electronic Systems, Institute for Basic Science, Pohang 790-784, Republic of Korea

ARTICLE INFO

Article history:
Available online 18 November 2014

Keywords:
Rashba states
Spin–orbit splitting
Tellurohalides
Angle-resolved photoemission

ABSTRACT

We present an overview of the new family of semiconductors BiTeX (X = I, Br, Cl) from the perspective of angle resolved photoemission spectroscopy. The strong band bending occurring at the surface potentially endows them with a large flexibility, as they are capable of hosting both hole and electron conduction, and can be modified by inclusion or adsorption of foreign atoms. In addition, their trigonal crystal structure lacks a center of symmetry and allows for both bulk and surface spin-split bands at the Fermi level. We elucidate analogies and differences among the three materials, also in the light of recent theoretical and experimental work.

1. Introduction

There has been a surge of interest for the consequences of spin-orbit (SO) coupling in solids [1,2] after the discovery of systems where the interaction is unexpectedly strong [3,4], with Rashba energies $E_R > 100$ meV and Rashba parameters $\alpha_R > 1$ eV·Å that are one to two orders of magnitude larger than in conventional semiconductor heterostructures [5]. Such numbers would potentially enable the operation of future room temperature spintronics devices. These novel systems, however, are usually the surfaces of bulk metals [6,7], or interfaces grown on metallic substrates [3,8], thus not suitable for technological applications, and also in the rare instances of semiconducting materials, they are artificially grown structures [4,9,10]. For these reasons the advent of an entirely new class of bulk semiconducting materials, the bismuth tellurohalides BiTeX (X = I, Br, Cl), possessing a wide (>100 meV) band gap and hosting bulk and surface states with a large SO splitting (Ref. [11] for BiTeI), has changed the perspective on the field and generated a burst of research activity.

The key point in common to these materials is a non-centrosymmetric crystal structure (see Fig. 1(a)) [12]. Their *c* axis is a chiral axis, and therefore they allow in their bulk for the characteristic lifting of the Kramers degeneracy caused by the SO interaction in lack of space-inversion symmetry. As a result, both their valence and conduction band states exhibit the characteristic splitting in energy and momentum. The three compound have quite similar electronic structures, with only quantitative differences [13]. They are also believed to be close to a transition topological phase, which could be induced by pressure [14]. The same SO interaction behind the Rashba effect is indeed also responsible for the band inversion in topological insulators, all of which contain one or more heavy elements. A topological state has also been reported at ambient pressure for BiTeCl [15], an observation which is however in contrast with all other experimental studies that have appeared to this point [16–18].

The experimental techniques of preference to investigate this new class of Rashba systems have been magnetotransport [19–21], which via the Shubunikov-de Haas effect can detect separately the oscillations of the inner and outer Fermi surfaces and therefore prove the presence of a non-trivial Berry's phase, optical spectroscopy [20,22–24], and angle-resolved photoemission (ARPES) [11,15–17,25–27]. The last one, main focus of this paper, is particularly powerful as it provides a direct view of the band structure of materials.

Fig. 1(b and c) shows the experimental ARPES band structure of BiTeI, measured along the $\overline{\Gamma K}$ high-symmetry direction, and two

* Corresponding author.
E-mail address: lmoreschini@lbl.gov (L. Moreschini).

http://dx.doi.org/10.1016/j.elspec.2014.11.004
0368-2048/

surface terminations (see below). In Fig. 1(b) the Fermi level lies in the conduction band (CB), approximately 350 meV above the minimum of the first (higher binding energy) electron-like band. Notice that some intensity from the hole-like valence states extends up to ~0.5 eV binding energy. This is not incompatible with an observed gap of 0.36 eV as observed by optical spectroscopy [22]. In fact, the intense electron-like band is not representative of the bulk CB, and is instead a state confined near the surface. Indeed, it does not show any dispersion when the photon energy is varied, i.e., it is independent of the wave vector k_z perpendicular to the surface [25,26]. The bulk CB minimum is found at ~0.2 eV, where a second pair of Rashba split bands is present. Their intensity is weak at the low (<50 eV) photon energy typically used in ARPES beamlines [26] or in laboratory sources [11], but it is already detectable at ~100 eV [25] and clearly visible in the soft x-ray range [26,27]. Moreover, in the sister compounds BiTeBr and BiTeCl an additional pair of bands was identified closer to the Fermi level, both by laser-based photoemission [16] and by circular dichroism [18].

Here lies a conceptual discrepancy in the interpretation of the ARPES data appeared up to this point. It has been proposed [11,16] that these electronic states represent quantized subbands confined in the accumulation layer induced by band bending at the surface, a situation well known to occur at the surfaces of semiconductors [28], transition metal oxides [29] or in topological insulators [30]. This scenario is sketched in Fig. 1(d). According to another interpretation (Fig. 1(e)) [25,26], the bands below the shallowest one (the bulk CB) are two-dimensional (2D) surface states originating from the first two trilayers of the crystal structure, a case not new in ARPES experiments on layered materials [31]. Although the two pictures are clearly distinct, the difference ensues from how the surface is modeled in calculations, and is therefore mainly a theoretical one. It is essentially impossible with photoemission to discriminate between these two cases, since a quantum well state induced by a surface band bending and a "true" surface state are both localized along the c axis and show therefore no photon energy dispersion. The two are also likely to be equivalent for any conceivable application, the only slight difference being that a true surface state is rigidly linked to the changes of band bending, e.g., resulting from surface doping, whereas the energy of the quantized subbands is linked in a non trivial way to the energy and the exact shape of the surface potential well.

2. Semiconductors with ambipolar conduction

A crucial aspect that went unnoticed in the initial work on BiTeI, the most thoroughly studied compound of the family, is that the succession of $(BiTe)^+$ blocks ionically bound to the $(X)^-$ halogen ones allows for two distinct surface terminations: Te and X. The Bi surface termination is energetically unfavorable since the electronegativity of Bi is slightly lower than that of Te and so the Bi atom is the more positively charged in the block, hence the more tightly bound by the ionic bond. Depending on the sample cleave, a charge accumulation or depletion region (Te and X terminations, respectively) can be generated at the surface. Both terminations are in general observed, due to the presence of stacking faults in the bulk crystal and to the random nature of cleaving. In some earlier reports the domains of either termination were smaller than the spot size of the incident light [11,26]. More recently, crystals with domains of the order of the hundreds of μm have been obtained at cleaved surfaces, enabling the separate measurements of a single termination in ARPES [25]. Electron depletion at the surface corresponds to an upward bending, and as a consequence the Fermi level lies within the valence band, as seen in Fig. 1(c) again for the case of BiTeI.

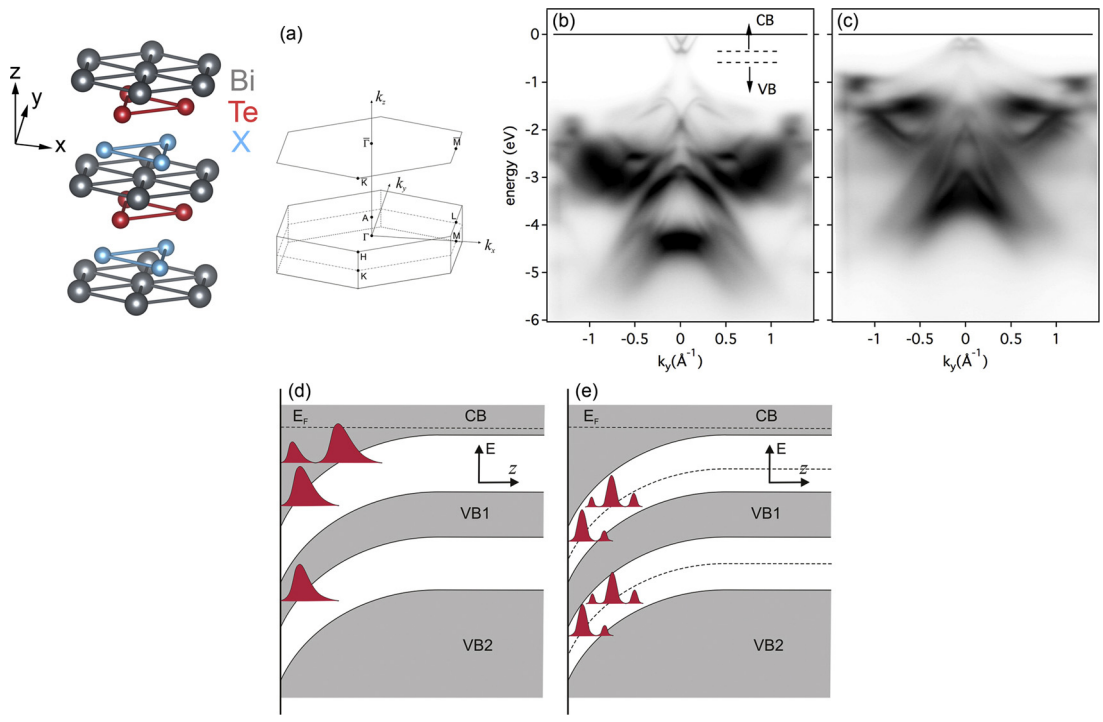

Fig. 1. (a) The trigonal layered structure of the BiTeX compounds, with Bi, Te and X planes alternating along the c axis. For X = Cl each BiTe block is staggered and rotated by 180° with respect to the next one, which causes a doubling of the unit cell size along c. The corresponding bulk and surface Brillouin zones (BZs) are also shown. Throughout this paper we will use as a convention k_x along $\overline{\Gamma M}$ and k_y along $\overline{\Gamma K}$. (b and c) The measured band structure for $h\nu = 93$ eV (close to the A point) at normal emission, for the Te and I surface, respectively. Notice the apparent difference in sharpness between bulk-related and surface-related spectral features. (d and e) Pictorial sketch of two different scenarios for the case of the Te termination. One calls for the formation of quantum well states inside the surface potential well (d), the other for surface states localized at different trilayer blocks of the crystal (e).

As an immediate consequence, these materials provide the possibility of ambipolar conduction, i.e., of both holes and electrons, depending on the induced band bending, together with the characteristic lifting of the spin degeneracy and the ensuing spin polarization provided by Rashba systems. This consists of two contours centered at the Γ point with spin polarization mainly contained in a plane parallel to the surface and opposite helicity, but depending on the compound the contours can evolve from circular to a more hexagonal shape which brings along a substantial P_z polarization with six-fold symmetry, breaking the simple Rashba spin geometry and less appealing for possible applications [11,13,25,26,32]. Furthermore, since these materials are layered quasi-2D systems, they naturally lend themselves to controlled layered growth, which makes it realistic to think of a patterned p–n junction on a common substrate [33,34].

The data shown in Fig. 1 were measured with $h\nu = 93$ eV, corresponding to a k_z value close to the A point of the 3D BZ for BiTeI. The sister compounds present slightly different values for the c axis lattice constant [12] ($c_{BiTeI} = 6.854$ Å, $c_{BiTeBr} = 6.487$ Å, $c_{BiTeCl} = 2 \times 6.198$ Å) and, in principle, different inner potentials for the same bands (we found $V_0 \simeq 8$ eV for BiTeI and $V_0 \simeq 6$ eV for BiTeBr, while $V_0 \simeq 9$ eV can be extracted from Ref. [17] for BiTeCl). However, for consistency and unless otherwise indicated, we use throughout this paper measurements at 93 eV which, in the photon energy range available on our beamlines, provides the most even intensity distribution amongst the electron-like states at the Fermi level. Fig. 2(a–c) shows as an example the variation in the relative intensity between the first and the second set of split surface bands for BiTeBr observed when the photon energy is changed by only 10 eV. The Fermi surfaces shown in Fig. 2(d and e) present indeed very distinct contours, representative of states confined (mainly) in the first and second layer, respectively. The strong intensity fluctuations with the photon energy are also sign that that these are far from being textbook surface states, for which strictly no intensity modulation with k_z is expected in the quasi free electron final state approximation, and that conversely they have a non negligible penetration depth into the solid. Note that the influence of the final states on the matrix elements, although responsible for numerous fluctuations of the dichroic signal with the photon energy [35] cannot account for the strong effect observed in Fig. 2 [36].

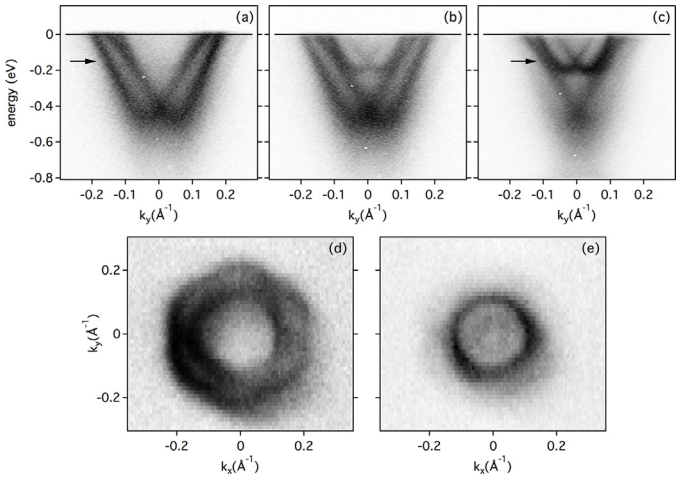

Fig. 2. Close-up of the bottom of the CB for a Te-terminated BiTeBr sample measured with $h\nu = 88$ eV (a), 93 eV (b) and 98 eV (c). (d and e) Fermi surfaces measured with $h\nu = 88$ eV and $h\nu = 98$ eV, and integrated over 15 meV around the Fermi level, showing the contour of the surface states for the first and second trilayer, respectively (see arrows). Both states do not show any k_z dispersion over more than one BZ (not shown). The bottom of the bulk CB is not visible at this photon energy, and lies even closer to the Fermi level, above the second trilayer state.

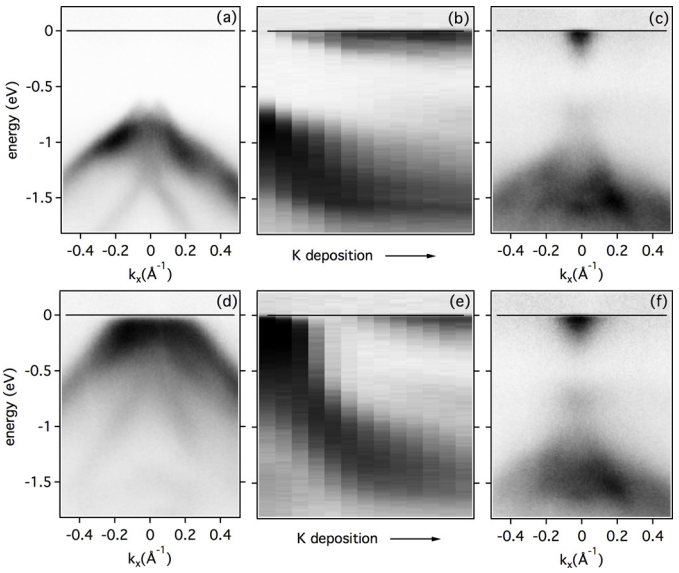

Fig. 3. Effect of K deposition on two Ag-intercalated BiTeBr samples, with Te termination (a–c) and Br termination (d–f). (a and d) show the band structure close to normal emission. (b and e) are stacks of energy distribution curves measured at normal emission during the K deposition, which directly visualize the downward drift of the bands. (c and f) are equivalent to (a and d) after the deposition process. The Ag-intercalated sample is in some sense the electron–hole symmetric of the stoichiometric one, with the Fermi level in the gap for the Te termination and inside the VB for the Br termination. The end point of the process is the same for both terminations, and corresponds roughly to the point where the bulk CB reaches the Fermi level.

Regardless of which description between Fig. 1(d) and (e) is closer to reality in this specific case, the electronic states at or in the vicinity of the Fermi level are for both terminations localized near the surface (the Cl termination in BiTeCl is an exception, as discussed later). This makes it simple to modify the band bending and effectively dope the compound by electrons or holes, since a relatively small amount of charge is sufficient to displace the Fermi level within the bulk band gap. An example is shown in the data of Fig. 3(a and b), measured on a sample of Ag-intercalated BiTeBr. The Ag atoms reduce the density of free charges in the material, thereby providing hole doping. As a consequence, the Fermi level lies below the CB in the Te termination, and into the VB in the Br termination, as opposed to stoichiometric BiTeBr, where the CB is partially populated in the Te-terminated surface (see Fig. 2) and the VB is fully occupied for the Br-terminated one. As common practice in cases when the dielectric constant allows an effective polarization of the material, a downward band bending can then be induced by deposition of K atoms on the surface (Fig. 3(c and d)). The deposition of alkali metals is a standard tool in ARPES for providing electron doping, and in insulators and semiconductors can be used for estimating the gap size [37]. By forming a K overlayer the VB and CB can be shifted down in a controlled way. Although the point of departure, i.e., the pristine surface, is very different, with a degenerate semiconductor for the Te termination and a p semiconductor for the Br termination, the arrival point is exactly the same. In other words, the K deposition is effective in bending the electronic bands of the solid down to the point where the bulk CB reaches the Fermi level, after which the charge required for pushing the bands even further is too large.

Since the analysis of the spectra in the VB and CB is complicated by the presence of surface- and bulk-related features, an easier way to evaluate the total energy difference in band bending provided by the two terminations is to compare the energy of the core levels for the two cases. This is done in Fig. 4, which yields $\Delta E \simeq 800$ meV,

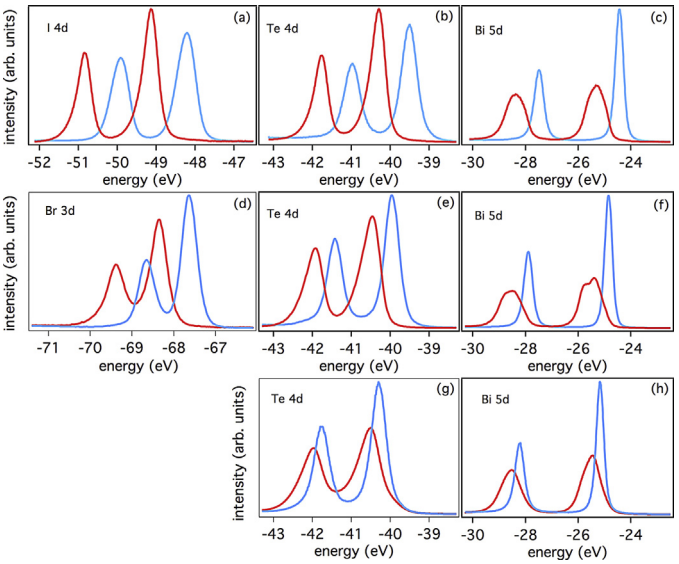

Fig. 4. Core level photoemission spectra measured with $h\nu = 120$ eV on the lowest energy *d* levels available for each element, for both terminations of BiTeI (a–c), BiTeBr (d–f) and BiTeCl (g and h). The Te and X terminations are in red and blue, respectively. The two spectra in each panel are normalized to the same total intensity. The slightly different branching ratio between panels of the same column is due to variations in the peak sharpness with the sample quality. The peaks of the red spectra present a typical asymmetric lineshape due to the metallic character of the Te terminations, as opposed to the symmetric peaks of the blue curves. The energy difference between each pair of peaks corresponds to the total band bending difference. As discussed in the text, such analysis cannot be done for BiTeCl, since the Cl surface is unstable and the band bending occurs together with a photochemistry effect which shifts the peaks in the opposite direction (to higher binding energies). (For interpretation of the references to color in this figure legend, the reader is referred to the web version of this article.)

$\Delta E \simeq 500$ meV and $\Delta E \simeq 200$ meV for X = I, Br and Cl, respectively. Note however that BiTeCl does not have a stable Cl termination. The surface states have been shown to fade quickly within seconds of exposure to the photon beam and the chemistry of the process causes the bands to drift downward [17]. This effect is superposed to the band bending at the Cl surface and has opposite sign. The energy difference between the core levels therefore cannot be used as it clearly underestimates the total upward band bending in the Cl termination. Another aspect deserves notice in Fig. 4, and namely the lineshape of the Bi 5*d* levels for the Te surface, which is much broader than for the X surface and even clearly shows, in the case of BiTeBr (Fig. 4(f)), two separate structures. This point was overlooked in our previous work [25], and it is probably the result of the migration of Bi atoms into the Te layer where they act as interstitial or substitutional defects, thus lowering the surface quality. We leave this question, of importance because ultimately related to the stability of a long range ordered surface, to spatial probes with atomic resolution such as scanning tunneling microscopy.

3. Methods

Single crystals of BiTeBr were grown by chemical vapor transport from a stoichiometric mixture of Bi, Te, and $BiBr_3$ sealed with HBr. The ampule was placed in a two-zone furnace held at 400° during growth. The synthesis of BiTeCl crystals involves a two-step process where single crystals of Bi_2Te_3 are produced and then mixed with excess $BiCl_3$ in a quartz ampoule placed vertically inside a muffle furnace. A temperature gradient of 400–440 °C from bottom to top of the ampoule, respectively, was applied [38]. BiTeI single crystals were obtained by melting in a sealed ampule a stoichiometric mixture of Bi, Te, and BiI_3 at 600 °C. The structure and

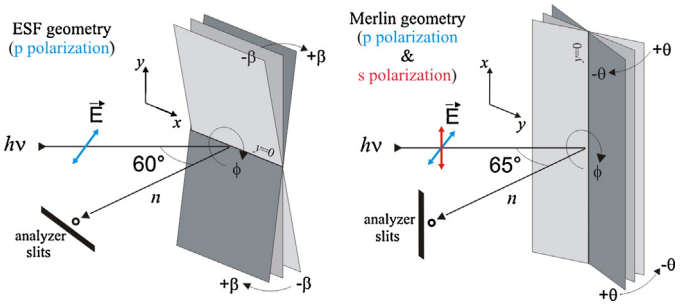

Fig. 5. The scattering geometry for the ESF and Merlin beamlines of the Advanced Light Source used for this work.

chemical composition of all compounds were confirmed by X-ray diffraction and energy dispersive x-ray spectroscopy.

The ARPES experiments were performed both at the Electronic Structure Factory (ESF) at beamline 7.0.1 and on the Merlin endstation at beamline 4.0.3 of the Advanced Light Source in Berkeley. The energy and momentum resolution were 30 meV and 0.1°, and 20 meV and 0.1°, respectively. The experimental geometry for the two endstations is sketched in Fig. 5. ESF data are used in Figs. 2(d and e) and 3, Merlin data in all the remaining ones. Whereas ESF provides only *p* linear polarization, Merlin allows for both *s* and *p* polarized light, but only *p* polarization was used for the data presented in this paper.

First-principles calculations of the three materials were performed within the density functional theory (DFT) framework employing the generalized gradient approximation (GGA) as implemented in the QUANTUM-ESPRESSO package [39]. Spin-orbit effects were accounted for using relativistic norm-conserving pseudopotentials acting on valence electron wavefunctions represented in the two-component spinor form [40]. We used an $8 \times 8 \times 6$ *k*-point mesh and a planewave kinetic energy cutoff of 50 Ryd. The convergence of results with respect to these parameters has been carefully checked. The surface states were investigated using 21 layers thick slab models with Te and halogen (I, Br, Cl) terminations. In order to reveal the surface states from the slab band structures, we projected the Kohn–Sham wavefunctions on atomic orbitals of the surface trilayer.

4. Discussion

Fig. 6 shows the band structures measured for the three BiTeX compounds and for both surface terminations. The sample azimuthal angle is such that we probe the $k_x = \overline{\Gamma}\overline{\mathrm{M}}$ direction. In real space the *x* direction corresponds to the in-plane next-nearest-neighbor bond which defines with the *z* axis a mirror plane for the crystal. Therefore the bulk band structure, which has only threefold symmetry, is not symmetric along k_x with respect to normal emission (it is along k_y, the nearest-neighbor direction). All the images present indeed a superposition of sharper symmetric bands, which come from the sixfold surface electronic structure, and broader asymmetric features, representative of the bulk. The results of the DTF calculations are shown in Fig. 7, separated into surface bands and surface-projected bulk bands. The position of the slab bands was adjusted by matching the value of the bulk potential to the potential in the middle of the slabs. DFT is not able to describe correctly the band bending effect at the surface and typically underestimates the band gap. As a consequence, the position of the surface states with respect to the Fermi level cannot be directly compared with the experimental value. With this exception, the band structure of the three compounds is well reproduced and so is the ambipolarity of the two terminations: close to the Fermi level

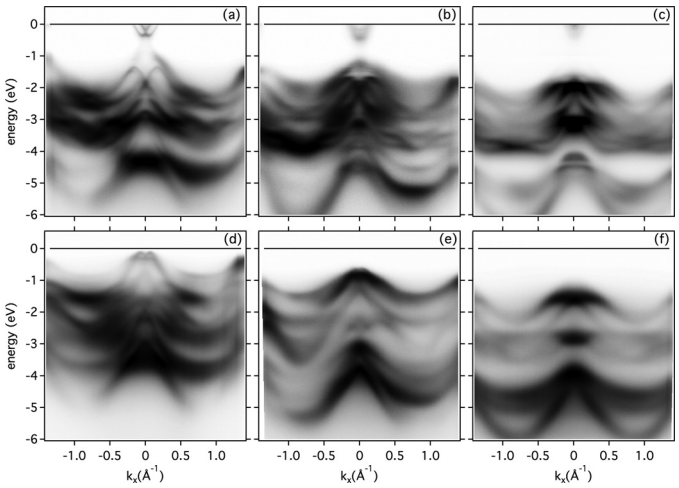

Fig. 6. Band structure measured along the k_x direction for a Te-terminated (a–c) and X-terminated (d–f) surface. From left to right, X = I, Br and Cl.

the Te termination presents electron-like surface states while the X-terminated surfaces all show hole-like ones. Many other states confined in the surface region are present much deeper (down to a few eV) into the VB, "trapped" in the gapped regions of the bulk band structure. This was noticed in previous work, both theoretically and experimentally [16,25,32].

Although in the experimental data the superposition of several features in the VB makes it difficult to tell apart all the different bands, it is apparent that the spin splitting is different for bulk and surface states, as it is different (larger) in the VB with respect to the CB. Both are consequence of the potential gradient ΔV at the surface. Even though it is established that the atomic potential gradient is the key ingredient for a large splitting in surface (Rashba–Bychkov) as in bulk (Rashba) states, for the Rashba–Bychkov effect also plays a role ΔV present within the topmost layers of crystal. How important is its role cannot be told *a priori* and has to be verified case by case. Whereas we have shown previously that the modification of ΔV by the deposition of an alkali metal on the Te surface of BiTeI has hardly any influence on the size of the splitting of the CB surface state [25], the observation of a larger splitting in the surface VB states occurring in the X-terminated samples fits with a calculated potential much steeper at the X surface than at the Te surface (Refs. [41], [32] and [13] for X = I, Br and Cl, respectively).

For the first CB surface state the computed Rashba parameters α_R, which can be extracted as $\alpha_R = 2E_R/k_0$ from the energy difference E_R between the crossing point and the band minimum and the momentum splitting k_0, are $\alpha_{R,I} = 2.20$ eV·Å, $\alpha_{R,Br} = 2.04$ eV·Å and $\alpha_{R,Cl} = 1.95$ eV·Å, and increase with the atomic number of the halogen element. The values from theory are to be compared with those extracted from ARPES, $\alpha_{R,I} \simeq 4.1$ eV·Å, $\alpha_{R,Br} \simeq 2.3$ eV·Å and $\alpha_{R,Cl} \simeq 1.9$ eV·Å, which are in turn within a 10% error bar with respect to those reported in Ref. [16]. The agreement is very good for X = Br, Cl and less good for X = I, as less good the agreement for BiTeI is also in the only other comparative DFT study [16] (Ref. [42] instead underestimates the Rashba parameter for X = Br,Cl and is more accurate for X = I, but the values reported there are estimated from the bulk bands and not directly calculated). The VB surface states present a larger departure from a parabolic dispersion and the extraction of α_R from the above formula is therefore inaccurate.

The trend of the splitting as extracted from the experiment is in line with a postulated inverse correlation to the bulk gap size [14], with BiTeI having the smallest gap and BiTeCl the largest. In this respect, note that the minimum gap in these compounds is found at the A point, edge of the BZ, for X = I, Br and at the Γ point for X = Cl due to the folding of the 3D BZ by the doubled periodicity along the c axis. The data of Fig. 6, measured with $h\nu = 93$ eV, are representative of A_5 for BiTeI, between Γ_5 and A_5 ($k_z \simeq 10.3\pi/c$) for BiTeBr and Γ_{10} for BiTeCl. Therefore they capture the minimum gap region for BiTeI and BiTeCl, but not for BiTeBr. The seemingly very large gap in BiTeCl (Fig. 6(c)) is due to the low intensity of the top of the valence band at this photon energy [17].

From the work done on this family of compounds up to this point, different factors seem to lead to different conclusions on the

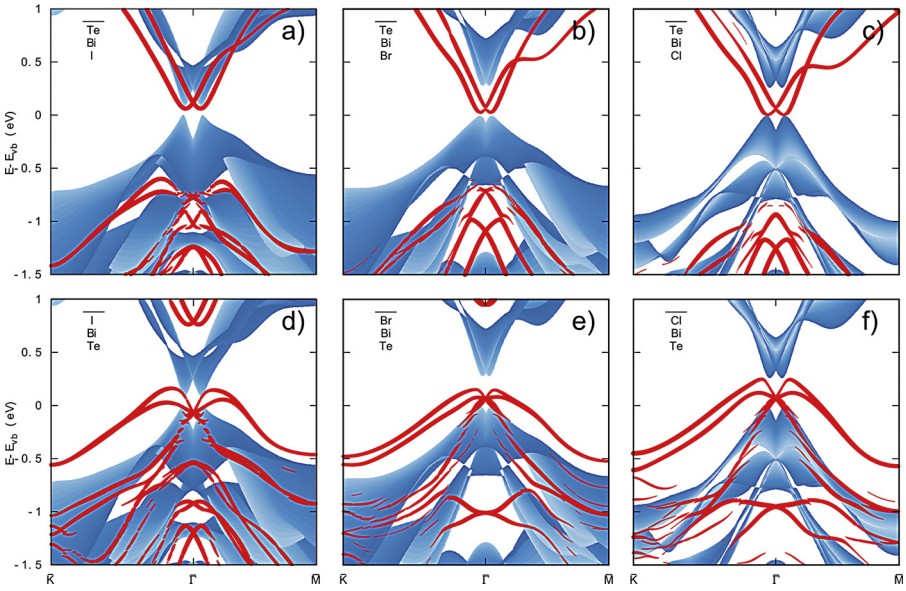

Fig. 7. Surface-projected slab band structures calculated from first principles and shown along the two high symmetry $\overline{\Gamma K}$ and $\overline{\Gamma M}$ directions of the surface BZ, with the same ordering of the panels as in Fig. 6 (remark though the different energy scale). The zero energy is set at the top of the bulk VB states. The red lines correspond to the slab bands with line thickness proportional to the wavefunction weight on the surface trilayer with (a–c) halogen and (d–f) Te terminations. Only states with more than 30% weight on the surface trilayer are shown. The blue shaded area show the surface-projected bulk band structure with the color intensity indicating k_z values ($k_z = 0$ – dark blue; $k_z = \pi/c$ – light blue). With this convention the figures contain information on the whole 3D BZ band structure. (For interpretation of the references to color in this figure legend, the reader is referred to the web version of this article.)

best candidate for possible future applications. Let alone the possibility of a topological phase [14], which has not been verified yet, from the point of view of the Rashba physics BiTeI would naively appear as the most natural choice, given the largest momentum splitting. However, the details of the band bending at the surface, which is about twice as steep in BiTeBr and BiTeCl [32], are such that the surface states in Te-terminated BiTeI are very close to the bulk states. Less than 200 meV separate the bottom of the surface state from the onset of the bulk CB, whereas this separation is about twice as large for the Br and Cl counterparts [16] and even a second pair of bands, from the second trilayer and fully non-degenerate with the CB, appears close to the Fermi level. BiTeCl has been argued to be the most promising of the three due a supposedly very isotropic dispersion of the CB surface state [13] which would yield a nearly pure "Rashba" $(P_x, P_y) = (\sin\theta, \cos\theta)$ spin polarization, with no P_z component. BiTeCl is also the most 2D of the family, and in fact barely any sign of threefold symmetry is visible in the data of Fig. 6(c and f). However, the only ARPES mapping published to this point [16] could not definitely exclude hexagonal warping of the Fermi surface, such as in Fig. 2(d) for BiTeBr. In addition, the instability of the Cl surface [17] hinders the possibility of ambipolar conduction in BiTeCl, and in general the quality of the published experimental data suggests that its synthesis is more delicate than for the two sister compounds. BiTeBr on the other hand has very close values for gap and spin splitting to BiTeCl, but does not present any obvious shortcoming. As we have shown here, its low energy states can also be easily switched from electrons to holes by extrinsic doping, without any apparent loss of surface quality, to the extent that ARPES can determine.

Acknowledgements

We acknowledge support by the Swiss NSF, namely through grants No. PP00P2-133552 (G.A. and O.V.Y) and PA00P21-36420 (L.M.). We thank Yeongkwan Kim and Beomyoung Kim for technical support on Merlin. The Advanced Light Source is supported by the Director, Office of Science, Office of Basic Energy Sciences, of the U.S. Department of Energy under Contract No. DE-AC02-05CH11231. Electronic structure calculations have been performed at the Swiss National Supercomputing Centre (CSCS) under project s515.

References

[1] E. Rashba, Sov. Phys. Solid State 2 (1960) 1109.
[2] Y. Bychkov, E. Rashba, JETP Lett. 39 (1984) 78.
[3] C.R. Ast, J. Henk, A. Ernst, L. Moreschini, M.C. Falub, D. Pacilé, P. Bruno, K. Kern, M. Grioni, Phys. Rev. Lett. 98 (2007) 186807.
[4] I. Gierz, T. Suzuki, E. Frantzeskakis, S. Pons, S. Ostanin, A. Ernst, J. Henk, M. Grioni, K. Kern, C.R. Ast, Phys. Rev. Lett. 103 (2009) 046803.
[5] J. Nitta, T. Akazaki, H. Takayanagi, T. Enoki, Phys. Rev. Lett. 78 (1997) 1335.
[6] G. Nicolay, F. Reinert, S. Hüfner, P. Blaha, Phys. Rev. B 65 (2001) 033407.
[7] Y.M. Koroteev, G. Bihlmayer, J.E. Gayone, E.V. Chulkov, S. Blügel, P.M. Echenique, P. Hofmann, Phys. Rev. Lett. 93 (2004) 046403.
[8] L. Moreschini, A. Bendounan, H. Bentmann, M. Assig, K. Kern, F. Reinert, J. Henk, C.R. Ast, M. Grioni, Phys. Rev. B 80 (2009) 035438.
[9] K. Sakamoto, H. Kakuta, K. Sugawara, K. Miyamoto, A. Kimura, T. Kuzumaki, N. Ueno, E. Annese, J. Fujii, A. Kodama, et al., Phys. Rev. Lett. 103 (2009) 156801.
[10] K. Sakamoto, T. Oda, A. Kimura, K. Miyamoto, M. Tsujikawa, A. Imai, N. Ueno, H. Namatame, M. Taniguchi, P.E.J. Eriksson, et al., Phys. Rev. Lett. 102 (2009) 096805.
[11] K. Ishizaka, M.S. Bahramy, H. Murakawa, M. Sakano, T. Shimojima, T. Sonobe, K. Koizumi, S. Shin, H. Miyahara, A. Kimura, et al., Nat. Mater. 10 (2011) 521.
[12] A. Shevelkov, E. Dikarev, R. Shpanchenko, B. Popovkin, J. Solid State Chem. 114 (1995) 379.
[13] S.V. Eremeev, I.A. Nechaev, Y.M. Koroteev, P.M. Echenique, E.V. Chulkov, Phys. Rev. Lett. 108 (2012) 246802.
[14] M.S. Bahramy, B.J. Yang, R. Arita, N. Nagaosa, Nat. Commun. 3 (2012) 679.
[15] Y.L. Chen, M. Kanou, Z.K. Liu, H.J. Zhang, J.A. Sobota, D. Leuenberger, S.K. Mo, B. Zhou, S.-L. Yang, P.S. Kirchmann, et al., Nat. Phys. 9 (2013) 704.
[16] M. Sakano, M.S. Bahramy, A. Katayama, T. Shimojima, H. Murakawa, Y. Kaneko, W. Malaeb, S. Shin, K. Ono, H. Kumigashira, et al., Phys. Rev. Lett. 110 (2013) 107204.
[17] G. Landolt, S.V. Eremeev, O.E. Tereshchenko, S. Muff, B. Slomski, K.A. Kokh, M. Kobayashi, T. Schmitt, V.N. Strocov, J. Osterwalder, et al., New J. Phys. 15 (2013) 085022.
[18] A. Crepaldi, F. Cilento, M. Zacchigna, M. Zonno, J.C. Johannsen, C. Tournier-Colletta, L. Moreschini, I. Vobornik, F. Bondino, E. Magnano, et al., Phys. Rev. B 89 (2014) 125408.
[19] H. Murakawa, M.S. Bahramy, M. Tokunaga, Y. Kohama, C. Bell, Y. Kaneko, N. Nagaosa, H.Y. Hwang, Y. Tokura, Science 342 (2013) 1490.
[20] C. Martin, E.D. Mun, H. Berger, V.S. Zapf, D.B. Tanner, Phys. Rev. B 87 (2013) 041104.
[21] C. Bell, M.S. Bahramy, H. Murakawa, J.G. Checkelsky, R. Arita, Y. Kaneko, Y. Onose, M. Tokunaga, Y. Kohama, N. Nagaosa, et al., Phys. Rev. B 87 (2013) 081109.
[22] J.S. Lee, G.A.H. Schober, M.S. Bahramy, H. Murakawa, Y. Onose, R. Arita, N. Nagaosa, Y. Tokura, Phys. Rev. Lett. 107 (2011) 117401.
[23] S. Bordács, J.G. Checkelsky, H. Murakawa, H.Y. Hwang, Y. Tokura, Phys. Rev. Lett. 111 (2013) 166403.
[24] M.K. Tran, J. Levallois, P. Lerch, J. Teyssier, A.B. Kuzmenko, G. Autès, O.V. Yazyev, A. Ubaldini, E. Giannini, D. van der Marel, et al., Phys. Rev. Lett. 112 (2014) 047402.
[25] A. Crepaldi, L. Moreschini, G. Autès, C. Tournier-Colletta, S. Moser, N. Virk, H. Berger, P. Bugnon, Y.J. Chang, K. Kern, et al., Phys. Rev. Lett. 109 (2012) 096803.
[26] G. Landolt, S.V. Eremeev, Y.M. Koroteev, B. Slomski, S. Muff, T. Neupert, M. Kobayashi, V.N. Strocov, T. Schmitt, Z.S. Aliev, et al., Phys. Rev. Lett. 109 (2012) 116403.
[27] M. Sakano, J. Miyawaki, A. Chainani, Y. Takata, T. Sonobe, T. Shimojima, M. Oura, S. Shin, M.S. Bahramy, R. Arita, et al., Phys. Rev. B 86 (2012) 085204.
[28] P.D.C. King, T.D. Veal, C.F. McConville, J. Zú niga Pérez, V. Mu noz Sanjosé, M. Hopkinson, E.D.L. Rienks, M.F. Jensen, P. Hofmann, Phys. Rev. Lett. 104 (2010) 256803.
[29] P.D.C. King, R.H. He, T. Eknapakul, P. Buaphet, S.-K. Mo, Y. Kaneko, S. Harashima, Y. Hikita, M.S. Bahramy, C. Bell, et al., Phys. Rev. Lett. 108 (2012) 117602.
[30] M.S. Bahramy, P.D.C. King, A. de la Torre, J. Chang, M. Shi, L. Patthey, G. Balakrishnan, P. Hofmann, R. Arita, N. Nagaosa, et al., Nat. Commun. 3 (2012).
[31] Y.J. Chang, L. Moreschini, A. Bostwick, G.A. Gaines, Y.S. Kim, A.L. Walter, B. Freelon, A. Tebano, K. Horn, E. Rotenberg, Phys. Rev. Lett. 111 (2013) 126401.
[32] S.V. Eremeev, I.P. Rusinov, I.A. Nechaev, E.V. Chulkov, New J. Phys. 15 (2013) 075015.
[33] C. Tournier-Colletta, G. Autès, B. Kierren, P. Bugnon, H. Berger, Y. Fagot-Revurat, O.V. Yazyev, M. Grioni, D. Malterre, Phys. Rev. B 89 (2014) 085402.
[34] C.J. Butler, H.-H. Yang, J.-Y. Hong, S.-H. Hsu, R. Sankar, C.-I. Lu, H.-Y. Lu, K.-H.O. Yang, H.-W. Shiu, C.-H. Chen, et al., Nat. Commun. 5 (2014).
[35] M. Ärrälä, J. Nieminen, J. Braun, H. Ebert, M. Lindroos, Phys. Rev. B 88 (2013) 195413.
[36] M. Mulazzi, G. Rossi, J. Braun, J. Minár, H. Ebert, G. Panaccione, I. Vobornik, J. Fujii, Phys. Rev. B 79 (2009) 165421.
[37] R. Comin, G. Levy, B. Ludbrook, Z.-H. Zhu, C.N. Veenstra, J.A. Rosen, Y. Singh, P. Gegenwart, D. Stricker, J.N. Hancock, et al., Phys. Rev. Lett. 109 (2012) 266406.
[38] J. Jacimovic, X. Mettan, A. Pisoni, R. Gaal, S. Katrych, L. Demko, A. Akrap, L. Forro, H. Berger, P. Bugnon, et al., Scr. Mater. 76 (2014) 69.
[39] P. Giannozzi, S. Baroni, N. Bonini, M. Calandra, R. Car, C. Cavazzoni, D. Ceresoli, G.L. Chiarotti, M. Cococcioni, I. Dabo, et al., J. Phys.: Condens. Matter (2009) 395502.
[40] A.D. Corso, A.M. Conte, Phys. Rev. B 71 (2005) 115106.
[41] S. Eremeev, I. Nechaev, E. Chulkov, JETP Lett. 96 (2012) 437.
[42] I.P. Rusinov, I.A. Nechaev, S.V. Eremeev, C. Friedrich, S. Blügel, E.V. Chulkov, Phys. Rev. B 87 (2013) 205103.